# Chapter 7

# Discovery of pyrazoline analogs through lead optimization strategy

# Chapter 7

**Discovery of pyrazoline analogs through lead optimization strategy**

## 7.1 Design strategy

The strategy for designing of multi-targetable pyrazoline derivatives bearing *N*-aryl piperazine scaffold, through the lead optimization-based approach, is depicted in **Figure 7.1**. It was noteworthy that the reported chalcone derivatives showed the inhibitory potential against the selected targets including, AChE, BuChE and BACE-1 along with inhibition of Aβ aggregation. Moreover, balanced inhibitory profile, against the selected targets, was exhibited by lead compound containing unsubstituted benzylpiperazine fragment and para-bromo substitution at the chalcone moiety. In the present study, we further optimized the chalcone scaffold to derive the pyrazole series with different substituents at the *N*-aryl piperazine moiety. Pyrazolines are stable and important class of heterocyclic compounds, constituting the structure of numerous therapeutic agents. The pyrazolines scaffold allows for several structural changes to the ring to obtain the compounds with diverse pharmacological activities. The scaffold has been extensively explored. It also exhibits favourable pharmacokinetic properties, including good oral bioavailability, metabolic stability, and suitable half-life that enhances its potential as therapeutic candidate. Importantly, the scaffold is reported to have a salutary effect in the treatment of AD through inhibition of AChE and Aβ plaques (201). Sari O. *et. al* reported the novel series of 2-pyrazoline derivatives as multifunctional agents with potential of ChEs inhibition, Aβ anti-aggregation and neuroprotection. The developed compounds exhibited potent and selective inhibition against BuChE, while compound **1a,** among series, showed dual inhibitory activity against AChE and BuChE. Further assessments showed significant reduction in the $A\beta_{1-42}$ aggregation levels along with the neuroprotective effect (202). Previously, we reported the analogs of pyrazole and spiropyrazoline as multifunctional agents for AD (135). The *de novo* fragment growing

strategy was utilized for the designing of novel 3,5-diarylpyrazoles and further hit optimization of spiropyrazoline derivatives was carried out as ChE inhibitors. Compound **2a** from the developed series showed potent inhibition against AChE and BuChE. It was also found to be safer on MC65 cells and decreased metal induced $A\beta_{1-42}$ aggregation (135). Sever B. *et. al* reported a series of thiazolyl-pyrazolines derivatives, designed on the basis of molecular hybridization of thiazole and pyarazoline moiety, and evaluated for efficacy by *in vitro* enzymatic assays. Compound **3a** was found to be the most promising derivative with significant effects on AChE and carbonic anhydrase (CA) inhibitory activity (203). Supuran *et.al* also reported the pyrazoline benzensulfonamides derivatives (**4a**) as carbonic anhydrase and AChE inhibitors with non-cytotoxic effect (204). Özdemir A. *et. al* designed and synthesised the 2-pyrazolines derivatives and examined their inhibitory effects against AChE and BuChE through *in vitro* and *in silico* studies. Compound **5a** exerted significant AChE inhibitory action and high BBB permeability (205). Abdelwahab *et. al* reported the novel pyrazoline derivatives (**6a**) specifically targeting AChE. In addition to the *in vitro* testing of the synthesised molecule, further *in silico* studies including molecular docking analysis and DFT calculations also demonstrated its activity (206). The *N*-aryl piperazine scaffold has been proven to be promising for its anti-AD activity along with the strong neuronal protection and anti-neuroinflammatory properties (126). Therefore, it was retained in the newly designed compounds with different substitutions at aryl moiety. Accordingly, a novel series of compounds has been synthesized and tested on different *in silico*, *in vitro* and *in vivo* biological parameters.

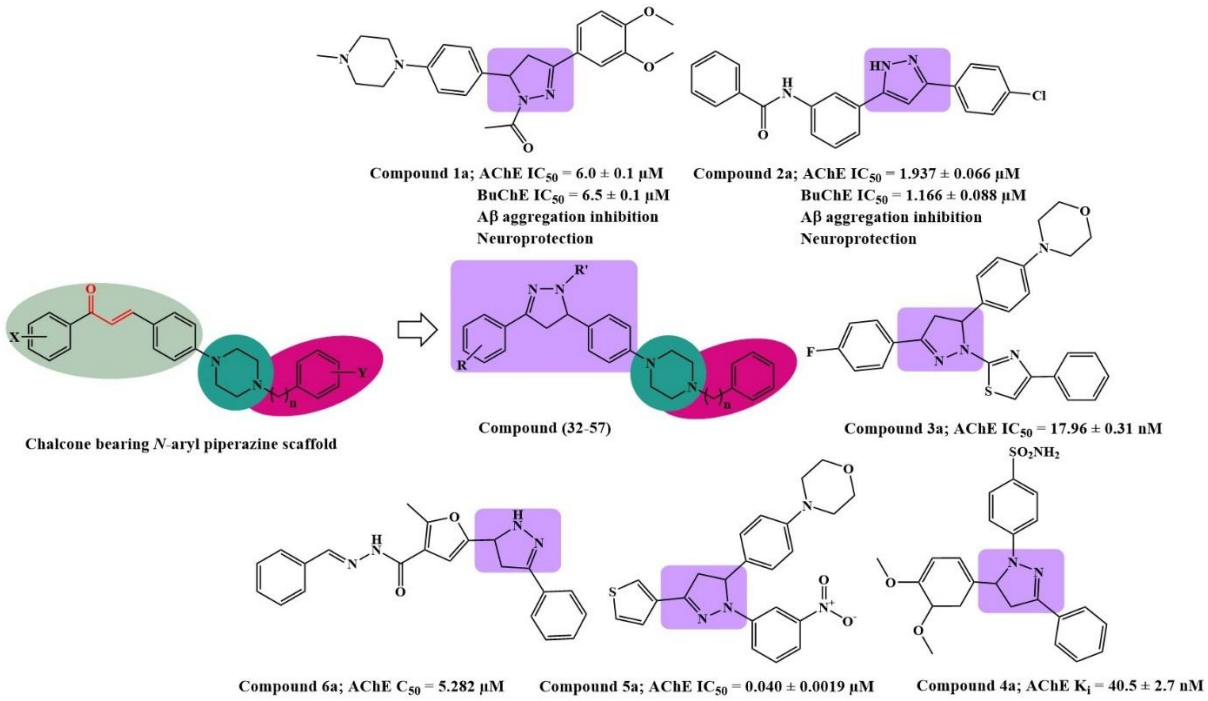


**Figure 7.1.** Design strategy of multi-target-directed ligand for AD.

## 7.2 Experimental procedures

### 7.2.1 Chemistry

The reagents were purchased from Sigma-Aldrich, Avera, BLD Pharm, Spectrochem, and Alfa Aesar. The precoated silica gel 60 F254 plates from Merck KGaA were utilized to perform thin layer chromatography to monitor the progress of the reaction. The visualization of spots was carried out by using ultraviolet light (254 nm) and iodine vapors. The synthesized compounds were purified by column chromatography (stationary phase: silica gel of 60-120 mesh size). The automated Bamstead Electrothermal apparatus was used to determine the melting point of the compounds. The $^{1}H$ and $^{13}C$ NMR spectra were recorded in $CDCl_3$ solvent on a Bruker Advance 500 & 125 MHz instrument with Tetramethylsilane (TMS) as the internal standard.

#### 7.2.1.1 General procedure for synthesis of compounds 4 – 5

In the dimethylformamide (DMF) 5 ml solvent, containing mixture of 4-Fluorobenzaldehyde (**1**) (1.0 equiv) and anhydrous $K_2CO_3$ (2.0 equiv), appropriate amount of *N*-aryl piperazine (**2-3**) (1.0 equiv) was added. The reaction mixture was refluxed for 12h at 115°C in a round-bottom flask with constant stirrer. The progress of the reaction was assessed on TLC plates. At the end, reaction mixture was transferred into ice water and the formed solid was filtered. Solid was washed with distilled water and further with few times with petroleum ether to get the pure product (**4-5)** in excellent yields.

#### 7.2.1.2 General procedure for synthesis of compounds 16 – 31

The compounds (**4-5**) (1.5 equiv) along with an appropriate substituted acetophenone (**6–15**) (1.0 equiv) was cooled in ethanol. Then, 2 ml aqueous solution of NaOH (2.5 M) was added dropwise. The obtained reaction mixture was stirred for 8–12 h at room temperature. On the completion of reaction, the precipitate was filtered and washed with cold ethanol to obtain crude product **16-31**.

#### 7.2.1.3 General procedure for synthesis of compounds 32 – 47

To stirred solutions of compounds **(16-31)** in ethanol (10 ml), hydrazine hydrate (10 eq.) was added. The reaction mixture was refluxed at 90-110$^0$C for 2h and progress was monitored by TLC. After the completion of the reaction, solvent was evaporated under reduced pressure. The precipitates were washed with ice-cold ethanol to yield final compounds of high purity (**32-47**).

***1-Phenyl-4-(4-(3-phenyl-4,5-dihydro-1H-pyrazol-5-yl)phenyl)piperazine*** **(32):**

Yellowish-white solid, 73% yield, M.P. 265-268 $^0$C, $^1$H NMR (500 MHz, , $CDCl_3$) δ 7.72 (d, *J* = 8.0 Hz, 1H), 7.52 (m, 2H), 7.42 (m, 3H), 7.34 (m, 4H), 7.02 (t, *J* = 1.4 Hz, 1H), 7.01 – 6.96 (m, 2H), 6.93 (m, 3H), 4.91 (t, *J* = 9.6 Hz, 1H), 3.52 – 3.46 (m, 1H),

3.45 – 3.38 (m, 8H), 3.09 (dd, *J* = 16.3, 8.5 Hz, 1H). $^{13}$C NMR (125 MHz, $CDCl_3$) δ 151.45, 151.19, 143.76, 129.23, 127.36, 126.63, 120.16, 116.39, 115.71, 113.99, 55.36 49.31, 48.78. 41.43.

***1-(4-(3-(2-Chlorophenyl)-4,5-dihydro-1H-pyrazol-5-yl)phenyl)-4-phenylpiperazine*** **(33):** Yellow solid, 76% yield, M.P. 245-260 $^0$C, $^1$H NMR (500 MHz, $CDCl_3$) δ 7.73 – 7.68 (m, 1H), 7.44 – 7.39 (m, 1H), 7.37 – 7.34 (m, 2H), 7.31 (dd, *J* = 12.9, 7.4 Hz, 4H), 7.01 (dd, *J* = 11.7, 8.4 Hz, 4H), 6.93 (t, *J* = 7.1 Hz, 1H), 4.92 (t, *J* = 9.6 Hz, 1H), 3.62 (dd, *J* = 16.6, 10.4 Hz, 1H), 3.37 (m, 8H), 3.26 (dd, *J* = 16.6, 8.9 Hz, 1H). $^{13}$C NMR (125 MHz, $CDCl_3$) δ 151.22, 150.87, 133.58, 132.48, 132.40, 130.53, 130.17, 129.62, 129.22, 127.31, 126.80, 120.16, 116.44, 116.40, 64.74, 49.40, 49.35, 43.86.

***1-(4-(3-(2,4-Dichlorophenyl)-4,5-dihydro-1H-pyrazol-5-yl)phenyl)-4-phenylpiperazine*** **(34):** Creamy-white solid, 72% yield, M.P. 158-161 $^0$C, $^1$H NMR (500 MHz, $CDCl_3$) δ 7.69 (d, *J* = 8.5 Hz, 1H), 7.44 (d, *J* = 2.1 Hz, 1H), 7.36 – 7.32 (m, 4H), 7.28 (dd, *J* = 8.5, 2.1 Hz, 1H), 7.02 (dd, *J* = 16.7, 8.3 Hz, 4H), 6.95 (t, *J* = 7.3 Hz, 1H), 4.92 (t, *J* = 9.3 Hz, 1H), 3.60 (dd, *J* = 16.6, 10.4 Hz, 1H), 3.38 (s, 8H), 3.23 (dd, *J* = 16.6, 9.0 Hz, 1H). $^{13}$C NMR (125 MHz, Chloroform-*d*) δ 151.09, 150.89, 149.58, 134.70, 133.40, 132.98, 130.97, 130.91, 130.31, 129.25, 127.31, 127.20, 120.32, 116.49, 64.85, 49.45, 49.32, 43.70.

***1-(4-(3-(3-Methoxyphenyl)-4,5-dihydro-1H-pyrazol-5-yl)phenyl)-4-phenylpiperazine*** **(35):** Creamy-white solid, 65% yield, M.P. 148-152 $^0$C, $^1$H NMR (500 MHz, $CDCl_3$) δ 7.27 – 7.14 (m, 6H), 7.11 (d, *J* = 7.1 Hz, 1H), 6.92 – 6.78 (m, 6H), 4.77 (t, *J* = 9.3 Hz, 1H), 3.75 (s, 3H), 3.33 (dd, *J* = 16.0, 10.9 Hz, 1H), 3.24 (s, 8H), 2.94 (dd, *J* = 16.1, 8.4 Hz, 1H). $^{13}$C NMR (125 MHz, $CDCl_3$) δ 158.72, 151.99, 150.83, 149.71, 135.76, 132.71, 129.17, 127.79, 127.18, 118.18, 117.30, 116.45, 115.32, 113.50, 108.99, 57.36, 55.42, 49.09, 49.07, 49.05, 41.38.

***1-(4-(3-(3-Nitrophenyl)-4,5-dihydro-1H-pyrazol-5-yl)phenyl)-4-phenylpiperazine***

**(36):** Whitish brown solid, yield − 91%, M.P.- °C $^{1}$H NMR (500 MHz, $CDCl_3$) δ 8.46 (s, 1H), 8.19 (d, *J* = 7.7 Hz, 1H), 8.06 (d, *J* = 7.5 Hz, 1H), 7.57 (t, *J* = 7.9 Hz, 1H), 7.30 (d, *J* = 10.8 Hz, 4H), 7.01 (d, *J* = 13.1 Hz, 4H), 6.93 (t, *J* = 6.8 Hz, 1H), 4.99 (t, *J* = 9.6 Hz, 1H), 3.49 (dd, *J* = 16.4, 10.6 Hz, 1H), 3.37 (s, 8H), 3.10 (dd, *J* = 16.2, 8.6 Hz, 1H). $^{13}$C NMR (125 MHz, $CDCl_3$) δ 148.61, 148.56, 134.89, 133.30, 129.47, 129.23, 127.17, 122.97, 120.66, 120.27, 116.50, 116.42, 64.31, 49.40, 49.27, 40.81.

***1-(4-(3-(4-Bromophenyl)-4,5-dihydro-1H-pyrazol-5-yl)phenyl)-4-phenylpiperazine***

**(37):** Yellow solid, 78% yield, M.P. 244-247 $^{0}$C, $^{1}$H NMR (500 MHz, $CDCl_3$) δ 7.51 (m, 4H), 7.34 (d, *J* = 7.4 Hz, 4H), 7.02 (m, 4H), 6.93 (m, 1H), 4.91 (t, *J* = 9.6 Hz, 1H), 3.45 (dd, *J* = 16.5, 10.9 Hz, 1H), 3.38 (s, 8H), 3.04 (dd, *J* = 16.2, 8.6 Hz, 1H). 13C NMR (125 MHz, $CDCl_3$) δ 151.46, 143.78, 131.70, 129.23, 127.46, 127.36, 127.23, 126.62, 120.17, 116.46, 116.39, 115.71, 64.05, 49.39, 49.32, 48.78, 40.98.

***1-(4-(3-(4-Chlorophenyl)-4,5-dihydro-1H-pyrazol-5-yl)phenyl)-4-phenylpiperazine***

**(38):** Faint yellow solid, 72% yield, M.P. 235-242 $^{0}$C, $^{1}$H NMR (500 MHz, $CDCl_3$) δ 7.62 (d, *J* = 8.3 Hz, 2H), 7.50 (d, *J* = 8.4 Hz, 4H), 7.37 (m, 2H), 7.29 (m, 1H), 6.92 (d, *J* = 7.2 Hz, 4H), 4.91 (t, *J* = 9.5 Hz, 1H), 3.51 (dd, *J* = 16.0, 10.9 Hz, 1H), 3.41 (s, 8H), 3.04 (dd, *J* = 16.3, 8.6 Hz, 1H). $^{13}$C NMR (125 MHz, $CDCl_3$) δ 151.46, 151.18, 143.79, 129.22, 128.75, 127.36, 127.22, 127.19, 126.61, 120.17, 116.45, 116.39, 115.70, 49.39, 49.32, 48.78, 41.05.

***1-(4-(3-(4-Methoxyphenyl)-4,5-dihydro-1H-pyrazol-5-yl)phenyl)-4-phenylpiperazine***

**(39):** Yellowish-white solid, 78% yield, M.P. 248-252 $^{0}$C, $^{1}$H NMR (500 MHz, $CDCl_3$) δ 7.66 (d, *J* = 8.2 Hz, 2H), 7.52 (m, 4H) 7.33 (m, 3H), 6.92 (m, 4H), 4.87 (t, *J* = 9.4 Hz, 1H), 3.59 (dd, *J* = 16.2, 10.6 Hz, 1H), 3.43 (s, 8H), 3.05 (dd, *J* = 16.3, 8.4 Hz, 1H). $^{13}$C

NMR (125 MHz, $CDCl_3$) δ 161.24, 151.45, 151.19, 143.76, 129.23, 127.36, 126.63, 120.16, 116.39, 115.71, 55.32, 49.31, 49.07, 48.78, 41.75.

***1-Benzyl-4-(4-(3-phenyl-4,5-dihydro-1H-pyrazol-5-yl)phenyl)piperazine*** **(40):** White solid, 93% yield, M.P. 159-162 $^0$C, $^1$H NMR (500 MHz, $CDCl_3$) δ 7.71 (d, *J* = 8.5 Hz, 2H), 7.43 – 7.36 (m, 7H), 7.32 (d, *J* = 6.9 Hz, 1H), 7.28 (d, *J* = 8.7 Hz, 2H), 6.91 (d, *J* = 8.7 Hz, 2H), 4.88 (t, *J* = 9.4 Hz, 1H), 3.63 (s, 2H), 3.45 (dd, *J* = 16.3, 10.6 Hz, 1H), 3.27 – 3.21 (m, 4H), 3.07 (dd, *J* = 16.3, 8.4 Hz, 1H), 2.68 – 2.64 (m, 4H). $^{13}$C NMR (125 MHz, $CDCl_3$) δ 151.33, 150.98, 133.68, 133.04, 129.35, 128.71, 128.54, 128.36, 127.32, 127.18, 126.03, 116.21, 63.87, 63.01, 52.98, 48.98, 41.16.

***1-Benzyl-4-(4-(3-(2-chlorophenyl)-4,5-dihydro-1H-pyrazol-5-yl)phenyl)piperazine*** **(41):** Yellow solid, 54% yield, M.P. 136-139 $^0$C, 1H NMR (500 MHz, $CDCl_3$) δ 7.72 – 7.67 (m, 1H), 7.43 – 7.39 (m, 3H), 7.37 (t, *J* = 7.4 Hz, 2H), 7.34 – 7.26 (m, 5H), 6.92 (d, *J* = 8.8 Hz, 2H), 4.89 (t, *J* = 9.6 Hz, 1H), 3.65 (s, 2H), 3.60 (dd, *J* = 16.6, 10.3 Hz, 1H), 3.26 (t, *J* = 4.9 Hz, 4H), 3.22 (d, *J* = 8.8 Hz, 1H), 2.70 – 2.69 (m, 4H). $^{13}$C NMR (125 MHz, $CDCl_3$) δ 150.89, 150.84, 133.29, 132.47, 132.41, 130.52, 130.15, 129.59, 129.45, 128.40, 127.24, 126.78, 116.24, 64.72, 62.88, 52.87, 48.83, 43.81.

***1-Benzyl-4-(4-(3-(2,4-dichlorophenyl)-4,5-dihydro-1H-pyrazol-5-yl)phenyl)piperazine*** **(42):** Light yellow solid, 84% yield, M.P. 137-139 $^0$C, $^1$H NMR (500 MHz, $CDCl_3$) δ 7.67 (d, *J* = 8.5 Hz, 1H), 7.43 – 7.35 (m, 5H), 7.33 – 7.26 (m, 4H), 6.91 (d, *J* = 8.8 Hz, 2H), 4.89 (t, *J* = 9.3 Hz, 1H), 3.64 (s, 2H), 3.58 (dd, *J* = 16.6, 10.4 Hz, 1H), 3.27 – 3.23 (m, 4H), 3.22 – 3.17 (m, 1H), 2.70 – 2.65 (m, 4H). $^{13}$C NMR (125 MHz, $CDCl_3$) δ 151.01, 149.56, 134.67, 132.96, 130.98, 130.89, 130.29, 127.38, 127.20, 116.19, 64.83, 62.94, 52.92, 48.88, 43.64.

***1-Benzyl-4-(4-(3-(3-methoxyphenyl)-4,5-dihydro-1H-pyrazol-5-yl)phenyl)piperazine*** **(43):** Creamy-white solid, 74% yield, M.P. 138-141 $^0$C**,** $^1$H NMR (500 MHz, $CDCl_3$) δ

7.38 (dt, *J* = 13.3, 6.5 Hz, 5H), 7.32 (dd, *J* = 7.2, 2.1 Hz, 2H), 7.30 – 7.25 (m, 2H), 7.21 (d, *J* = 7.6 Hz, 1H), 6.90 (d, *J* = 8.7 Hz, 2H), 4.87 (t, *J* = 8.5 Hz, 1H), 3.86 (s, 3H), 3.65 (s, 2H), 3.43 (dd, *J* = 16.3, 10.6 Hz, 1H), 3.30 – 3.19 (m, 4H), 3.05 (dd, *J* = 16.3, 8.4 Hz, 1H), 2.71 – 2.64 (m, 4H). $^{13}$C NMR (125 MHz, $CDCl_3$) δ 159.71, 151.30, 150.87, 134.34, 133.75, 129.51, 128.40, 127.47, 118.78, 116.28, 115.18, 110.50, 63.87, 62.87, 55.31, 52.85, 48.83, 41.21.

***1-Benzyl-4-(4-(3-(3-nitrophenyl)-4,5-dihydro-1H-pyrazol-5-yl)phenyl)piperazine* (44):** Yellow solid, 82% yield, M.P. 152-154 $^0$C, $^1$H NMR (500 MHz, $CDCl_3$) δ 8.37 (m, 2H), 8.28 (dt, *J* = 7.5, 1.5 Hz, 1H), 7.93 (dt, *J* = 7.5, 1.5 Hz, 1H), 7.71 (t, *J* = 7.5 Hz, 1H), 7.34 – 7.32 (m, 4H), 7.26 – 7.21 (m, 3H), 6.78 (m, 2H), 4.93 (t, *J* = 9.4 Hz, 1H), 3.51 (m, 2H), 3.25 – 3.15 (m, 2H), 3.10 (m, 4H), 2.65 (m, 4H). $^{13}$C NMR (125 MHz, $CDCl_3$) δ 150.78, 149.98, 146.24, 138.59, 135.87, 133.23, 129.02, 128.70, 128.52, 127.71, 127.37, 127.18, 124.24, 119.09, 113.40, 62.07, 57.36, 52.66, 49.30, 41.25.

***1-Benzyl-4-(4-(3-(4-bromophenyl)-4,5-dihydro-1H-pyrazol-5-yl)phenyl)piperazine* (45):** Yellowish-white solid, 76% yield, M.P. 168-170 $^0$C, $^1$H NMR (500 MHz, $CDCl_3$) δ 7.53 (q, *J* = 8.6 Hz, 4H), 7.38 (dt, *J* = 14.9, 7.3 Hz, 5H), 7.25 (d, *J* = 8.6 Hz, 2H), 6.90 (d, *J* = 8.6 Hz, 2H), 4.88 (t, *J* = 9.1 Hz, 1H), 3.64 (s, 2H), 3.40 (dd, *J* = 16.3, 10.7 Hz, 1H), 3.29 – 3.22 (m, 4H), 3.02 (dd, *J* = 16.3, 8.5 Hz, 1H), 2.71 – 2.65 (m, 4H). $^{13}$C NMR (125 MHz, $CDCl_3$) δ 150.95, 150.16, 133.42, 131.98, 131.67, 129.43, 128.39, 127.45, 127.14, 122.67, 116.25, 64.03, 62.89, 48.83, 40.93.

***1-Benzyl-4-(4-(3-(4-chlorophenyl)-4,5-dihydro-1H-pyrazol-5-yl)phenyl)piperazine* (46):** White solid, 64% yield, M.P. 164-168 $^0$C, $^1$H NMR (500 MHz, $CDCl_3$) δ 7.61 (d, *J* = 8.7 Hz, 2H), 7.42 (d, *J* = 7.4 Hz, 2H), 7.38 – 7.31 (m, 5H), 7.30 – 7.22 (m, 2H), 6.94 – 6.85 (m, 2H), 4.93 – 4.81 (t, *J* = 9.3 Hz, 1H), 3.69 (s, 2H), 3.41 (dd, *J* = 16.3, 10.6 Hz, 1H), 3.33 – 3.20 (m, 4H), 3.02 (dd, *J* = 16.1, 8.4 Hz, 1H), 2.72 (m, 4H). $^{13}$C NMR (125

MHz, $CDCl_3$) δ 150.79, 150.18, 134.44, 133.62, 131.51, 129.59, 129.03, 128.73, 128.47, 127.16, 116.36, 63.99, 52.73, 41.01.

***1-Benzyl-4-(4-(3-(4-methoxyphenyl)-4,5-dihydro-1H-pyrazol-5-yl)phenyl)piperazine*** **(47):** Yellowish-white solid, 67% yield, M.P. 173-175 $^0$C, $^1$H NMR (500 MHz, $CDCl_3$) δ 7.65 (d, *J* = 8.8 Hz, 2H), 7.41 – 7.35 (m, 4H), 7.31 (d, *J* = 6.9 Hz, 1H), 7.27 (d, *J* = 8.7 Hz, 2H), 6.92 (dd, *J* = 18.0, 8.8 Hz, 4H), 4.84 (t, *J* = 9.6 Hz, 1H), 3.85 (s, 3H), 3.62 (s, 2H), 3.41 (dd, *J* = 16.2, 10.5 Hz, 1H), 3.26 – 3.18 (m, 4H), 3.04 (dd, *J* = 16.2, 8.4 Hz, 1H), 2.68 – 2.62 (m, 4H). $^{13}$C NMR (125 MHz, $CDCl_3$) δ 160.16, 151.38, 150.93, 133.81, 129.34, 128.35, 127.49, 127.31, 127.18, 125.83, 116.20, 113.98, 63.72, 63.00, 55.34, 52.98, 48.99, 41.38.

**7.2.1.4 General procedure for synthesis of compounds 48 – 57**

To a stirred solution of selected compounds from **32-47** in acetonitrile (5 ml), acetyl chloride or benzoyl chloride was added drop-wise with stirring at room temperature. Then catalytic amount of TEA was added and the reaction mixture was stirred for further 2 hours to afford the corresponding acetylated compounds 48-57 in good yield.

***1-(5-(4-(4-Benzylpiperazin-1-yl)phenyl)-3-phenyl-4,5-dihydro-1H-pyrazol-1-yl)ethan-1-one*** **(48):** Off white solid, yield - 91%, M.P.- 159–161 °C, $^1$H NMR (500 MHz, $CDCl_3$) δ 7.80 – 7.72 (m, 2H), 7.64 (s, 2H), 7.47 – 7.39 (m, 6H), 7.14 (d, *J* = 8.2 Hz, 2H), 6.82 (d, *J* = 8.2 Hz, 2H), 5.53 (dd, *J* = 11.6, 4.3 Hz, 1H), 4.12 (s, 2H), 3.73 (dd, *J* = 17.6, 11.8 Hz, 1H), 3.53 (s, 4H), 3.16 (d, *J* = 4.3 Hz, 1H), 3.17 – 3.12 (m, 4H), 2.41 (s, 3H). $^{13}$C NMR (125 MHz, $CDCl_3$) δ 168.86, 153.97, 149.06, 134.64, 131.39, 131.22, 130.36, 129.23, 128.77, 126.84, 126.63, 126.56, 117.33, 61.14, 59.45, 51.41, 46.87, 42.21, 22.06.

***(5-(4-(4-Benzylpiperazin-1-yl)phenyl)-3-phenyl-4,5-dihydro-1H-pyrazol-1-yl)(phenyl)methanone*** **(49):** Off white solid, yield − 84%, M.P.- 186–188 °C, $^1$H NMR (500 MHz, $CDCl_3$) δ 7.69 – 7.62 (m, 4H), 7.56 – 7.42 (m, 6H), 7.35 – 7.23 (m, 7H), 6.83 – 6.77 (m, 2H), 5.59 (dd, *J* = 11.1, 4.6 Hz, 1H), 3.61 – 3.52 (m, 2H), 3.38 (m, 2H), 3.03 (m, 4H), 2.78 (t, *J* = 7.1 Hz, 2H), 2.66 (t, *J* = 7.1 Hz, 2H). $^{13}$C NMR (125 MHz, $CDCl_3$) δ 165.04, 152.39, 150.76, 138.05, 135.01, 134.79, 133.83, 132.51, 130.38, 129.24, 128.81 – 128.51 (m), 128.42, 128.20, 127.22, 116.84, 66.14, 63.26, 53.02, 49.57, 38.96.

***1-(5-(4-(4-Benzylpiperazin-1-yl)phenyl)-3-(2,4-dichlorophenyl)-4,5-dihydro-1H-pyrazol-1-yl)ethan-1-one*** **(50):** White solid, yield − 87%, M.P.- 184–186 °C, $^{1}$H NMR (500 MHz, $CDCl_3$) δ 7.76 – 7.64 (m, 3H), 7.51 – 7.42 (m, 4H), 7.32 (dd, *J* = 8.4, 1.9 Hz, 1H), 7.15 (d, *J* = 8.1 Hz, 2H), 6.84 (d, *J* = 8.2 Hz, 2H), 5.52 (dd, *J* = 11.8, 4.3 Hz, 1H), 4.22 (s, 2H), 3.89 (dd, *J* = 18.1, 11.8 Hz, 1H), 3.61 (s, 4H), 3.30 (dd, *J* = 18.1, 4.4 Hz, 1H), 3.12 – 3.11 (m, 4H), 2.38 (s, 3H). $^{13}$C NMR (125 MHz, $CDCl_3$) δ 169.09, 152.43, 148.90, 136.26, 134.53, 133.70, 131.09, 130.76, 130.27, 129.40, 129.12, 127.43, 126.88, 117.56, 60.91, 59.73, 51.15, 46.55, 44.81, 21.96.

***(5-(4-(4-Benzylpiperazin-1-yl)phenyl)-3-(2,4-dichlorophenyl)-4,5-dihydro-1H-pyrazol-1-yl)(phenyl)methanone*** **(51):** Off white solid, yield - 82%, M.P.- 172–175 °C, $^{1}$H NMR (500 MHz, $CDCl_3$) δ 7.97 (d, *J* = 7.5 Hz, 2H), 7.72 – 7.63 (m, 3H), 7.51 – 7.44 (m, 5H), 7.42 (t, *J* = 7.5 Hz, 2H), 7.29 (m, 1H), 7.28 – 7.22 (m, 2H), 6.85 (d, *J* = 8.3 Hz, 2H), 5.75 (dd, *J* = 11.7, 4.8 Hz, 1H), 4.20 (s, 2H), 3.94 (dd, *J* = 18.1, 11.8 Hz, 1H), 3.61 (d, J = 24.4 Hz, 4H), 3.44 (s, 2H), 3.34 (dd, *J* = 18.1, 4.9 Hz, 1H), 2.96 (d, J = 12.3 Hz, 2H). $^{13}$C NMR (125 MHz, $CDCl_3$) δ 153.06, 148.88, 136.30, 134.45, 133.66, 131.61, 131.29, 131.23, 130.85, 130.28, 130.08, 129.99, 129.40, 129.00, 127.82, 127.71, 127.44, 127.02, 117.56, 117.47, 77.32, 61.00, 60.85, 46.46, 44.22.

***1-(5-(4-(4-Benzylpiperazin-1-yl)phenyl)-3-(3-methoxyphenyl)-4,5-dihydro-1H-pyrazol-1-yl)ethan-1-one*** **(52):** Off white solid, yield - 85%, M.P.- 175–177 °C, $^{1}$H NMR (500 MHz, $CDCl_3$) δ 7.46 (dt, *J* = 7.5, 1.5 Hz, 1H), 7.35 – 7.29 (m, 1H), 7.30 – 7.24 (m, 5H), 7.24 – 7.18 (m, 2H), 7.14 (t, *J* = 1.5 Hz, 1H), 6.93 (m, 1H), 6.83 – 6.77 (m, 2H), 5.51 (dd, *J* = 7.6, 6.7 Hz, 1H), 3.82 (s, 2H), 3.61 - 3.51 (m, 2H), 3.45 (dd, *J* = 12.5, 7.0 Hz, 1H), 3.40 (dd, *J* = 12.4, 7.1 Hz, 1H), 3.03 (t, *J* = 7.1 Hz, 4H), 2.64 (t, *J* = 7.1 Hz, 4H), 2.38 (s, 2H). $^{13}$C NMR (125 MHz, $CDCl_3$) δ 170.30, 158.45, 152.99, 150.29, 138.20, 134.28, 133.20, 128.70, 128.51, 127.84, 127.63, 127.49, 122.39, 115.65, 113.22, 111.43, 62.76, 62.02, 55.41, 52.91, 49.30, 40.34, 20.87.

***(5-(4-(4-Benzylpiperazin-1-yl)phenyl)-3-(3-methoxyphenyl)-4,5-dihydro-1H-pyrazol-1-yl)(phenyl)methanone*** **(53):** White solid, yield − 85%, M.P.- 175–177 °C, $^{1}$H NMR (500 MHz, $CDCl_3$) δ 7.98 (d, *J* = 7.3 Hz, 2H), 7.71 – 7.63 (m, 2H), 7.50 – 7.40 (m, 6H), 7.33 (d, *J* = 8.1 Hz, 1H), 7.30 (s, 2H), 7.26 (d, *J* = 8.2 Hz, 2H), 7.08 (d, *J* = 6.2 Hz, 2H), 7.00 – 6.94 (m, 1H), 5.76 (dd, *J* = 11.5, 4.6 Hz, 1H), 4.26 (s, 2H), 3.91 – 3.86 (m, 1H), 3.82 (s, 3H), 3.78 – 3.72 (m, 1H), 3.52 (dd, *J* = 48.3, 12.0 Hz, 4H), 3.27 (d, *J* = 11.6 Hz, 2H), 2.81 – 2.69 (m, 2H). $^{13}$C NMR (125 MHz, $CDCl_3$) δ 166.42, 159.75, 154.71, 134.16,

132.50, 131.57, 130.33, 130.00, 129.83, 129.42, 127.68, 127.29, 119.42, 118.54, 112.06, 60.78, 50.38, 45.89.

***1-(5-(4-(4-Benzylpiperazin-1-yl)phenyl)-3-(4-bromophenyl)-4,5-dihydro-1H-pyrazol-1-yl)ethan-1-one*** **(54):** White solid, yield − 92%, M.P.- 168–170 °C, $^{1}$H NMR (500 MHz, $CDCl_3$) δ 7.63 (s, 2H), 7.60 (d, *J* = 8.4 Hz, 2H), 7.55 (d, *J* = 8.3 Hz, 2H), 7.42 (s, 3H), 7.11 (d, *J* = 7.6 Hz, 2H), 6.81 (d, *J* = 7.4 Hz, 2H), 5.53 (dd, *J* = 7.4, 6.5 Hz, 1H), 4.12 (s, 2H), 3.69 (dd, *J* = 17.4, 11.9 Hz, 1H), 3.51 (s, 4H), 3.22 – 3.08 (m, 4H), 2.39 (s, 3H). $^{13}$C NMR (125 MHz, $CDCl_3$) δ 168.86, 152.91, 149.15, 134.38, 131.98, 131.27, 130.35, 129.80, 129.22, 128.07, 126.79, 124.63, 117.32, 59.63, 51.47, 46.85, 22.05.

***(5-(4-(4-Benzylpiperazin-1-yl)phenyl)-3-(4-bromophenyl)-4,5-dihydro-1H-pyrazol-1-yl)(phenyl)methanone*** **(55):** White solid, yield - 81%, M.P.- 183–185 °C, $^{1}$H NMR (500 MHz, $CDCl_3$) δ 7.77 – 7.71 (m, 2H), 7.68 – 7.62 (m, 2H), 7.62 – 7.56 (m, 2H), 7.52 – 7.45 (m, 3H), 7.32 – 7.22 (m, 5H), 7.29 – 7.23 (m, 2H), 6.82 – 6.78 (m, 2H), 5.64 (dd, *J* = 7.6, 6.4 Hz, 1H), 3.61 – 3.50 (m, 2H), 3.34 (dd, *J* = 12.5, 7.0 Hz, 1H), 3.26 (dd, *J* = 12.5, 7.0 Hz, 1H), 3.01 (m, 4H), 2.66 (m, 4H). $^{13}$C NMR (125 MHz, $CDCl_3$) δ 165.93, 151.94, 150.29, 138.17, 135.06, 134.21, 132.10, 131.82, 131.60, 129.21, 128.82, 128.70, 128.50, 128.41, 127.64, 127.49, 124.87, 113.17, 64.29, 61.57, 52.98, 49.60, 40.49.

***1-(5-(4-(4-Benzylpiperazin-1-yl)phenyl)-3-(4-chlorophenyl)-4,5-dihydro-1H-pyrazol-1-yl)ethan-1-one*** **(56):** Off white solid, yield − 86%, M.P.- 163–165 °C, $^{1}$H NMR (500 MHz, $CDCl_3$) δ 7.68 (d, *J* = 8.2 Hz, 4H), 7.45 (s, 3H), 7.40 (d, *J* = 8.2 Hz, 2H), 7.13 (d, *J* = 7.2 Hz, 2H), 6.82 (d, *J* = 6.7 Hz, 2H), 5.54 (dd, *J* = 7.3, 6.4 Hz, 1H), 4.16 (s, 2H), 3.70 (dd, *J* = 17.2, 12.0 Hz, 1H), 3.56 (s, 4H), 3.37 – 2.87 (m, 5H), 2.40 (s, 3H). $^{13}$C NMR (126 MHz, $CDCl_3$) δ 168.85, 152.80, 149.01, 136.30, 131.43, 129.91, 129.32, 129.04, 127.87, 126.84, 117.47, 61.07, 51.39, 46.73, 42.14, 22.05.

***(5-(4-(4-Benzylpiperazin-1-yl)phenyl)-3-(4-chlorophenyl)-4,5-dihydro-1H-pyrazol-1-yl)(phenyl)methanone*** **(57):** Off white solid, yield - 83%, M.P.- 184-186 °C, $^{1}$H NMR (500 MHz, Chloroform-*d*) δ 7.70 – 7.64 (m, 2H), 7.62 – 7.56 (m, 2H), 7.52 – 7.46 (m, 2H), 7.48 – 7.42 (m, 3H), 7.36 – 7.28 (m, 5H), 7.26 – 7.22 (m, 2H), 6.84 – 6.78 (m, 2H), 5.58 (dd, *J* = 7.4, 6.5 Hz, 1H), 3.62 – 3.52 (m, 2H), 3.35 (dd, *J* = 12.5, 7.0 Hz, 1H), 3.27 (m, 1H), 3.03 (m, 4H), 2.65 (m, 4H). $^{13}$C NMR (125 MHz, $CDCl_3$) δ 165.93, 151.74, 150.29, 139.19, 138.12, 135.09, 134.16, 132.08, 131.07, 129.21, 129.03, 128.69, 128.60, 128.51, 128.41, 127.64, 127.50, 113.17, 64.29, 61.71, 52.98, 49.52, 40.49.

### 7.2.2 *In-vitro* cholinesterase inhibition assay

The anti-cholinesterase activities of all the synthesized derivatives (**32-57**) were assessed by using previously reported protocols of modified Ellman colorimetric assay with minor modifications (134, 181, 182). In assay, Cholinesterase preferentially catalyzes the hydrolytic cleavage of thiolated substrates to produce thiocholine, which reduces the 5,5-dithio-bis-(2- nitrobenzoic acid) (DTNB) to provide the yellow color product that can be detected at 415 nm (207). The cholinesterase enzymes, *ee*AChE (CAS No. 9001–08-1) and *eq*BuChE (CAS No. 9000–81-5) was procured from Sigma-Aldrich, DPZ and rivastigmine were used as standard compounds. Briefly, the stock solutions of all the test compounds were made in biological grade DMSO solvent and further dilutions were prepared in the PBS. The assay method involved, first incubation of 50 µl of AChE (0.22 U/ml) or BuChE (0.06 U/ml) with test or standard compound (10 µl) in 96-well plates for the period of 30 min. Then after incubation, 30 µl of the substrate viz. ATCI (15 mM) or BTCI (15 mM) was added and the mixture was incubated for 30 min. Finally, 160 µl of DTNB (1.5 mM) was added to each well and absorbance was measured at of 415 nm using a 96-well microplate reader (Synergy HTX, BioTek, USA). The blank control included all the components except the enzymes i.e., *ee*AChE or *eq*BChE. All the assays were performed in triplicate and repeated independently at least two–three times. The absorbance data was used to calculate the percentage inhibition by the g expression: [(Ac − Ai)/Ac] × 100, where Ai and Ac is the absorbance in the presence and absence of the inhibitors respectively. The nonlinear regression log inhibitor concentration vs normalized response curves were used to graphically determine the $IC_{50}$ values of all the compounds examined using GraphPad Prism 5.01.

### 7.2.3 *In-vitro* blood-brain barrier permeation assay

In order to evaluate the preliminary brain permeability, test compounds were subjected to the parallel artificial membrane permeation assay-BBB (PAMPA-BBB), a well-established *in vitro* model using reported protocol with minor modifications (183). Concisely, the bottom surface of porous filter disks of acceptor plates was coated with porcine brain lipid (20 mg/ml in dodecane). The desired dilution of test compounds (500 µM) and equilibrium standard of each test compound along with blank control were prepared. In the assay, the acceptor plate was filled with 300 ul of PBS. To the wells of the donor plate (pore size = 0.45 mm, Merck Millipore), 200 µl of test compounds (500 µM) were added in duplicate. Then, the donor plate was kept into the acceptor plate wells carefully and incubated for the period of 18 h. After the completion of incubation period, donor plates were carefully removed. Absorbance of the compounds in the acceptor wells along with the prepared equilibrium standard of each test compound and permeability and blank control were recorded using a microplate reader. The recorded absorbance spectrum from wavelength of 200 nm to 500 nm in 10 nm intervals were used to determine the absorbance of the test compounds. Pe value was calculated by using the expression: Pe = C × -In (1- ODA/ ODE) cm/s, where ODA = absorbance of acceptor, ODE = equilibrium standard absorbance and if the experiment is running for 18 hrs, then C = $7.72 \times 10^{-6}$. The results are presented as the mean ± SD.

### 7.2.4 *h*BACE-1 inhibition assay

The BACE-1 inhibitory potential of the selected lead molecules was evaluated by FRET-based fluorometric assay using BACE-1 detection kit (CS0010, Sigma Aldrich, India) (185). The assay was performed as per the protocol mentioned in the catalogue and reported earlier (126). Further, percentage inhibition activity was calculated by using the

expression: [(IFo - IFi)/IFo] 100. Where, IFi and IFo represent fluorescence intensities in the presence and absence of inhibitor respectively.

### 7.2.5 Self-induced and AChE-induced Aβ$_{1-42}$ aggregation inhibition

Thioflavin T assay was used to evaluate the self and *ee*AChE-induced Aβ$_{1-42}$ aggregation inhibition activity of compound **48** (113). The lyophilized aliquot of Aβ$_{1-42}$ purchased from Cayman was dissolved in PBS and stored at - 80°C. Working solutions of the Aβ$_{1-42}$ were prepared in the PBS. Firstly, the stock solution of the test compound **48** was prepared in the DMSO and then final required dilutions of 5 µM, 10 µM, and 20 µM were prepared in PBS. Then, for the assay, the concentration ratios of Aβ$_{1-42}$: compound **48** (10:5, 10:10; and 10:20 µM) were selected (126, 186). In the self-induced Aβ$_{1-42}$ aggregation inhibition assay, Aβ$_{1-42}$ (10 µl; 10 µM) was incubated for 48 h with or without compound **48** (10 µl; 5 µM, 10 µM, and 20 µM). After completion of incubation period, Thioflavin T (178 µl, 20 µM) was added and the fluorescence intensities were measured at 450 nm (excited) and 485 nm (emission), immediately. In *ee*AChE-induced Aβ$_{1-42}$ aggregation inhibition assay, Aβ$_{1-42}$ (2 µl; 10 µM) and *ee*AChE (16 µl; 230 µM) were incubated for 48 h in the presence and absence of compound **48** (2 µl; 5 µM, 10 µM, and 20 µM). Then, Thioflavin T (178 µl; 20 µM) was added and fluorescence intensities were recorded (same as in self-induced). Statistical analysis was performed using one-way ANOVA followed by the Newman-Keuls post hoc test.

### 7.2.6 Molecular docking

Molecular docking studies of both *R* & *S*-configuration lead compound **48** with AChE (4EY7) (187) and BACE-1 (2VKM) (188) were carried out to gain insight into the binding mode interactions (203, 208). Autodock tools were used by employing Lamarckian Genetic Algorithm (LGA). The specified PDB was downloaded and protein were prepared in the Discovery Studio client version and ligands were prepared in the

Chem 3D. The perimeters for grid generation were selected based on the active sites of the protein structure. The genetic algorithms (GA) runs were fixed to 100 and other default docking parameters were used, followed by employing LGA. Then, the grid parameter file (gpf) and docking parameter file (dpf) were generated. The interaction of protein-ligand was visualized by using Discovery studio visualizer software.

### 7.2.7 Molecular dynamics

GROMACS 2020 package with the CHARMM-36M force field was applied to perform the molecular dynamics simulation studies for the timescale of 100 ns (188, 209). The docked protein-ligand complexes of the *R* & *S*-configuration of lead compound **48** with AChE were used to run the simulation (210, 211). At first, CHARMM-GUI web server was used to generate the topology files for the ligands with their respective complexes. The TIP3P model was used for the solvation of the protein-ligand complexes and periodic boundary conditions across all directions were applied. Monte Carlo ion placing method utilised to neutralized the excessive charge present on the complexes by adding the calculated number of $Na^+$ and $Cl^-$ ions. Then, energy minimization was performed with 5000 steps of the steepest descent algorithm. The LINCS algorithm was used to constrained all the present hydrogen bonds (212). The system was equilibrated with NVT and NPT ensembles for the period of 1ns using the leap-frog integrator. On the completion of the equilibration, the complexes were submitted to isobaric and isothermally controlled production run of 100 ns. The normal temperature of 310.15 K and pressure about 1 bar were monitored throughout the production run using velocity-rescaling and Parrinello-Rahman pressure methods, respectively. The produced trajectories, Root mean square deviation (RMSD), Root means square fluctuation (RMSF), inter-hydrogen bond, SASA, and RoG of the complexes were analysed (189).

### 7.2.8 *In vivo* biological evaluations

#### 7.2.8.1 Animals, housing, and ethical approval

Adult Swiss albino mice of either sex was procured and acclimatized in an animal room for 7 days (12:12 h dark/light cycle at 25 ± 2°C) at the animal house facilities of Department of Pharmaceutical Engineering & Technology, IIT (BHU). All the animal experiments were carried out as per the approved protocols (approval no. IIT(BHU/IAEC/2024/I/033) by the Institutional Animal Ethical Committee (IAEC), IIT (BHU), Varanasi.

#### 7.2.8.2 Acute oral toxicity studies

Compound 48 were tested for acute oral toxicity studies according to OECD 423 guidelines. The female albino mice were used for the toxicity test. As per the guidelines, mice were divided into two different groups (n = 3), where group I administered with vehicle alone (control group) and group II administered with compound **48** (300 mg/kg, po) single dose. Animals were monitored for next 14 days for toxic symptoms, change in body weight, food intake, behavioural changes, and mortality. All the mice were sacrificed on 14th day and organs were collected. The transverse sections (15 μm) of tissue sections were made using cryostat and mounted on the glass slide. The sections were stained with hematoxylin and eosin and examined microscopically.

#### 7.2.8.3 Behavioural studies

##### 7.2.8.3.1 Drugs and chemicals

Drugs i.e., DPZ HCl (CAS No. 120011-70-3) and Scopolamine HCl (CAS No. 55-16-3) were procured from Sigma-Aldrich. ACh ELISA kit was purchased from Krishgen Bio Systems, India. The other reagents used in studies were procured from commercial suppliers.

#### 7.2.8.3.2 Drug preparation and treatment protocols

Freshly prepared the solution of scopolamine (3 mg/ kg), DPZ (5 mg/kg), and then compound **48** were made in 0.3 % sodium carboxy methyl cellulose suspension (5, 10, and 20 mg/kg). The experimental animals were grouped as, n=6 into (i) Control group, (ii) Scopolamine (3 mg/kg, i.p.), (iii) Compound **48** (5 mg/kg, p.o.), (iv) Compound **48** (10 mg/kg, p.o.), (v) Compound **48** (20 mg/kg p.o.) (vi) DPZ (5 mg/kg, p.o.). Test compound **48** along with standard drug DPZ were administered daily for up to 7 days. On the last day (seventh day) animals were administered with the scopolamine except control group after 30 min of dosing of drug. The control group were administered with only vehicles. All the animals were put through the Y maze test after 15 min of the vehicle or scopolamine administration.

#### 7.2.8.3.3 Y-maze test

The widely used Y-maze test was performed to assess the spatial working and exploratory behaviour in rodents (133). The three-dimensional horizontal maze set apart by 120° apparatus consisted of three identical arms labelled as A, B, and C. The experimental groups including, control, scopolamine, compound **48** (2.5, 5 and 10 mg/kg) and DPZ (5 mg/kg). The control group was administered with 0.5% sodium carboxy methyl cellulose, whereas compound **48** and DPZ was administered to respective groups for 7 days. On the seventh day, scopolamine was injected intraperitoneally to all the animals except the control group. Then, after 30 min of scopolamine administration, spatial working memory was assessed using the Y-maze apparatus. In testing, at first each of the animal was placed at the centre of three arms (A, B, and C) and allowed for free movement for the period of 8 min. The video camera recording was carried out for each mice entry into the specified arm. The recorded data was analysed and % of alternation was calculated. The mice entered successively into three different arms (ABC, ACB, BAC, BCA, CAB,

and CBA) was considered for the spontaneous alternation (SA) determination. The following formula was used to determine the percentage alternation: % spontaneous alternation = [(number of alternations/total arm entries) − 2] X 100. GraphPad Prism 5.1 and Microsoft Excel version 20 were used to analyze experimental datasets and presented as mean ± SD. Statistical analysis was performed using one-way ANOVA followed by the Newman-Keuls post hoc test.

**7.2.8.4 *Ex-vivo* biochemical analysis**

On the completion of the behavioural experiment, mice were sacrificed via cervical dislocation. The brains were removed, and the hippocampus and cortex parts region were carefully isolated and homogenized using a glass homogenizer in 12.5 mM PBS (pH 7.4). The obtained homogenates were centrifuged for 30 minutes at 7000 rpm at 4°C, and the supernatants were collected for biochemical analysis. ACh activity was measured using an acetylcholine ELISA kit (Krishgen Biosystems, India). AChE activity, a cholinergic marker, was assessed by using a modified version of Ellman's colorimetric method. The protocol provided by the manufacturer and previously reported method was used to carried out the analysis and method thereof can be found here (7). The participation of CAT enzyme carried out the conversion of hydrogen peroxide ($H_2O_2$) into water and oxygen. The phenomena are used to estimate the CAT activity as per the reported protocol described by Sinha. The mixture for assay consists of 50 µl of PBS (0.1 M; pH 7.4), 5% dichromate/acetic acid solution (100 µl; 1:3 v/v), 50 µl of $H_2O_2$, and 50 µl of brain supernatant. Concisely, in the 96-well plate, brain supernatant (50 µl), PBS (50 µl), and 50 µl of $H_2O_2$ were incubated for 1 min at 37°C. On the completion of incubation, the solution of the dichromate/acetic acid solution (150 µl) was added followed by boiling for 10 min at 100°C, and thereafter absorbance measured at 570 nm. Estimation of an oxidative stress biomarker, MDA that involved in lipid peroxidation was determined with

the thiobarbituric acid reactive substance (TBARS) assay. Briefly, 8.1% sodium lauryl sulphate (0.2 ml), 0.8% aqueous thiobarbituric acid (TBA) solution (1.5 ml), and 20% glacial acetic acid (1.5 ml) were added to the brain homogenate (0.2 ml). The mixture prepared by adding deionized water up to 4.0 ml and heated for 60 min at 95°C. The mixture was cooled with tap water and mixture of n-butanol and pyridine mixture (15:1 v/v; 5 ml) and 1 ml of distilled water were added and centrifuged. The separated organic layer (200 µl) was added to a 96-well plate and absorbance was measured at 532 nm well microplate reader. GraphPad Prism 5.1 and Microsoft Excel version 20 were used to analyze experimental datasets and presented as mean ± SD. Statistical analysis was performed using one-way ANOVA followed by the Newman-Keuls post hoc test.

## 7.3 Results and discussion

### 7.3.1 Chemistry

The designed compounds **32-57** were synthesised as depicted in the scheme (**Scheme 7.1)**. The synthesis of compounds **16-31** was carried out as described previously (126). The reaction of 4-fluorobenzaldehye **(1)** with *N*-arylpiperazine **(2–3)** in the presence of a strong base potassium carbonate ($K_2CO_3$) underwent nucleophilic substitution reaction to give intermediates (**4-5**) (190). The second intermediates **(16-31)** were synthesized by the reacting the obtained intermediate **(4-5)** of substituted *N*-arylpiperazine, having free aldehyde group, with the substituted acetophenone (**6-15**). In the reaction, acetone and aldehyde undergo the base-catalyzed condensation in presence of base i.e., NaOH (2.5 M) solution that afforded the alpha–beta unsaturated carbonyl compounds. Further, to a stirred solution of compounds **(16-31)** in ethanol, hydrazine hydrate (10 eq.) was added. The reaction mixture was refluxed for 4 h at 90°C and progress of reaction was monitored by TLC. Once the reaction was complete, solvent was evaporated and product was dried under reduced pressure. The precipitates were washed with ice-cold ethanol to yield final

substituted pyrazoline scaffolds containing *N*-arylpiperazine compounds **(32-47)** in good yield. The lead compounds among the **32-47** were further subjected for the acetylation with acetyl chloride and benzoyl chloride in the presence of triethylamine to afford desired compounds **48-57**. The obtained product was further purified and characterized through NMR $^{1}H$ (500 MHz), $^{13}C$ (125 MHz) and HRMS spectra. The appendix contains the spectral characterization details of the representative lead molecules.

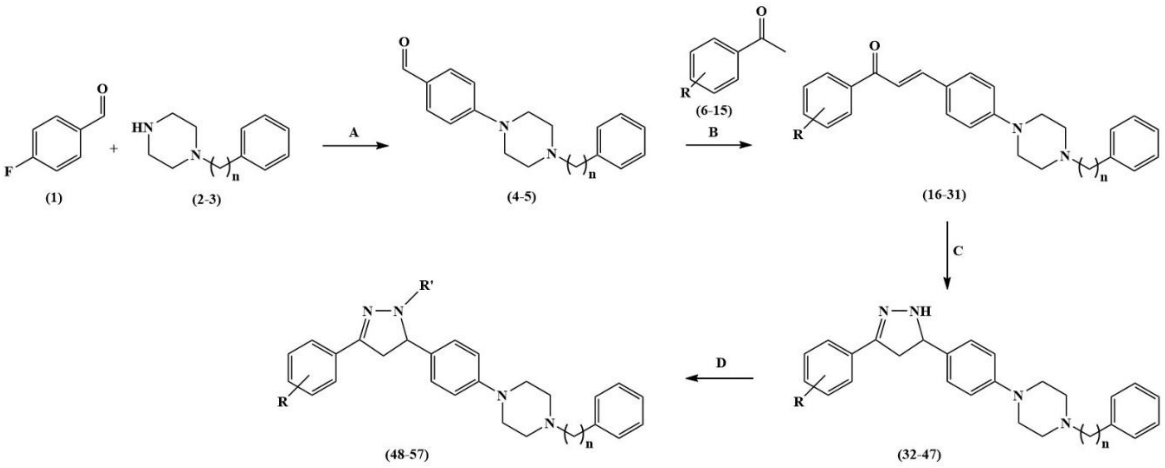


**Scheme 7.1.** [a] Reagents and conditions: (A) 4-Fluorobenzaldehyde (**1**) 1.0 equiv, substituted *N*-arylpiperazine (**2-3**) 1.2 equiv, Potassium carbonate 2.0 equiv, DMF, 125° C, 12 h; (B) Compound **4-5** 1.5 equiv, substituted acetophenone (**6-15**) 1.0 equiv, 2 ml of 2.5 M NaOH solution, ethanol, rt, overnight. (C) Compound **16-31** 1.0 equiv, 10 ml of ethanol, hydrazine hydrate (5 eq.) reflux, 2 h. (D) Compound **32-47** 1.0 equiv, benzoyl/acetyl chloride (1.5 eq.), 0.2 ml Triethylamine, THF, reflux, 5 h.

### 7.3.2 *In-vitro* cholinesterase inhibition

The inhibition of cholinesterase enzyme can restore the depleted cholinergic function in AD through consequently increasing the accessibility of ACh at the synaptic cleft. Another important enzyme, BuChE exhibits secondary action that could compensate for AChE in hydrolyzing central ACh.

**Table 7.1:** Structures, cholinesterase (*ee*AChE and *eq*BuChE) inhibitory profile, PAMPA-BBB assay, and BACE-1 inhibitory activity of tested compounds.

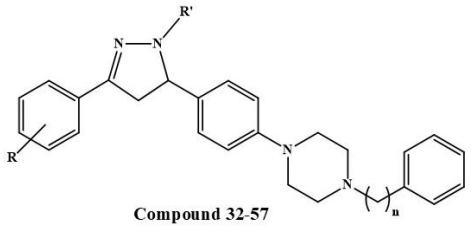


Compound 32-57

| Com No. | R | R' | n | $IC_{50}$ (μM) [a] or % Inhibition[b] | | Pe ($10^{-6}$cm $s^{-1}$) | BACE-1 % Inhibition[d] |
|---|---|---|---|---|---|---|---|
| | | | | ***ee*AChE** | ***eq*BuChE** | | |
| **32** | **H** | - | 0 | 25.25 ± 1.36 % | 29.13 ± 1.18 % | - | - |
| **33** | **2-Chloro** | - | 0 | 28.56 ± 0.38 % | na | - | - |
| **34** | **2,4-Chloro** | - | 0 | 5.40 ± 0.211 | na | 5.55 ± 0.448 | - |
| **35** | **3-Methoxy** | - | 0 | 24.23 ± 0.62 % | 27.67 ± 1.54 % | - | - |
| **36** | **3-Nitro** | - | 0 | 14.19 ± 1.42 % | 38.07 ± 1.86 % | - | - |
| **37** | **4 -Bromo** | - | 0 | 19.44 ± 0.37 % | na | - | - |
| **38** | **4-Chloro** | - | 0 | 15.92 ± 1.17 % | na | - | - |
| **39** | **4-Methoxy** | - | 0 | 29.67 ± 1.93 % | na | - | - |
| **40** | **H** | - | 1 | 4.63 ± 0.665 | 2.11 ± 0.259 | 5.21 ± 0.151 | - |
| **41** | **2-Chloro** | - | 1 | 4.70 ± 0.258 | 1.85 ± 0.254 | 7.29 ± 0.813 | - |
| **42** | **2,4-diChloro** | - | 1 | 2.99 ± 0.534 | 1.59 ± 0.096 | 7.33 ± 0.089 | - |
| **43** | **3-Methoxy** | - | 1 | 3.73 ± 0.473 | 2.344 ± 0.173 | 5.38 ± 0.046 | - |
| **44** | **3-Nitro** | - | 1 | 8.28 ± 1.781 | 24.26 ± 1.59 % | - | - |
| **45** | **4-Bromo** | - | 1 | 5.61 ± 0.421 | 5.293 ± 0.332 | - | - |
| **46** | **4-Chloro** | - | 1 | 4.78 ± 0.469 | 29.28 ± 1.67 % | - | - |
| **47** | **4-Methoxy** | - | 1 | 8.34 ± 1.824 | 27.87 ± 0.19 % | - | - |
| **48** | **H** | $COCH_3$ | 1 | 2.89 ± 0.706 | 0.151 ± 0.089 | 7.28 ± 0.474 | 36.64 ± 1.343 |
| **49** | **H** | $COC_6H_5$ | 1 | 4.96 ± 0.381 | 3.329 ± 0.893 | - | - |
| **50** | **2,4-Chloro** | $COCH_3$ | 1 | 4.04 ± 0.523 | 0.663 ± 0.322 | - | - |
| **51** | **2,4-Chloro** | $COC_6H_5$ | 1 | 5.08 ± 0.401 | 3.690 ± 0.927 | - | - |
| **52** | **3-Methoxy** | $COCH_3$ | 1 | 2.19 ± 0 .140 | 3.380 ± 0.352 | 12.12 ± 0.728 | - |
| **53** | **3-Methoxy** | $COC_6H_5$ | 1 | 4.086 ± 0.415 | 0.247 ± 0.072 | 7.76 ± 0.609 | 26.19 ± 1.635 |
| **54** | **4-Bromo** | $COCH_3$ | 1 | 3.393 ± 0.916 | 1.079 ± 0.300 | 5.75 ± 0.636 | 41.02 ± 1.290 |
| **55** | **4-Bromo** | $COC_6H_5$ | 1 | 4.891± 0.311 | 4.843 ± 0.491 | - | - |
| **56** | **4 -Chloro** | $COCH_3$ | 1 | 2.831 ± 0.528 | 0.569 ± 0.031 | 6.87 ± 0.444 | 34.64 ± 1.198 |
| **57** | **4-Chloro** | $COC_6H_5$ | 1 | 4.143 ± 0.317 | 3.824 ± 0.245 | - | - |
| **-** | **DPZ** | - | - | 0.076 ± 0.0032 | - | 11.39 ± 0.569 | - |
| **-** | **RIVA** | - | - | - | 0.92 ± 0.014 | - | - |

[a] Results are reported as the mean $IC_{50}$ ± SD (n = 3).

[b] % inhibition for AChE & BuChE was calculated at 20 μM concentration of inhibitors.

[c] $IC_{50}$ coefficients of determination ($R^2$)

[d] BACE-1 % Inhibition was calculated at 10 μM concentration of inhibitors. n.a. not active.

Thus, concurrent inhibition of AChE and BuChE is considered as an intriguing approach for the development of anti-AD agent (194). Accordingly, all the novel synthesized derivatives (**32-57**) were evaluated for their dual inhibitory potency and DPZ was used as a positive reference standard. All the 2-pyrazoline derivatives demonstrated the increase in cholinesterase inhibitory activity as compared to the previously reported chalcone derivatives. The pyrazoline scaffold was retained as a core nucleus in all the derivatives with and without *N*-substituted acetyl or benzoyl derivatives. Among all the tested compounds (**32-57**), compounds (**32–39**) substituted with benzyl piperazine showed a more pronounced inhibitory potential than their respective phenyl piperazine derivatives. In phenyl piperazine derivatives, compound **34** showed the better cholinesterase inhibitory activity than the other derivatives. Surprisingly, most of the compounds with *N*-benzyl piperazine substituted derivatives were found to be more potent against BuChE than AChE. Pyrazoline series without *N*-substitution (**40-47**) exhibited moderate inhibitory potential against AChE and BuChE. The di-chloro-substituted (**42**; AChE $IC_{50}$ = 2.99 ± 0.534 μM; BuChE $IC_{50}$ = 1.590 ± 0.096 μM) and meta-methoxy substituted (**43**; AChE $IC_{50}$ = 3.73 ± 0.473 μM; BuChE $IC_{50}$ = 2.344 ± 0.173 μM) derivatives turned out to be potent AChE and BuChE inhibitors. Whereas, para-methoxy substitution (**47**; AChE $IC_{50}$ = 8.34 ± 1.824 μM; BuChE $IC_{50}$ = 27.87 ± 0.19 %) showed lower inhibition. Some reports suggested that *N*-substitution on pyrazoline scaffold may improve the potency against AChE and BuChE (201, 205, 213). On further evaluation, compounds (**48–57)** with *N*-acetylated pyrazoline containing

benzyl piperazine moiety showed better activities. Compound **48** (AChE $IC_{50}$ = 2.89 ± 0.706 μM; BuChE $IC_{50}$ = 0.151± 0.089 μM) and **56** (AChE $IC_{50}$ = 2.831 ± 0.528 μM; BuChE $IC_{50}$ = 0.569 ±0.031 μM) with *N*-acetyl substitution at pyrazoline bearing benzylpiperazine fragment exhibited potent inhibition among all the synthesized derivatives. This supported the intent that the presence of the *N*-acetylation on pyrazoline scaffold (**48–57**) may be responsible for the better inhibition against ChEs.

### 7.3.3 *In-vitro* blood-brain barrier permeation assay

The major prerequisite for the molecule targeting AD is the BBB permeability. Accordingly, selected synthesized derivatives screened for the assessment of BBB permeation by using widely used parallel artificial membrane permeation assay (PAMPA), as described previously (123, 183). The reference permeability (Pe) values of nine commercially available drugs were used as a benchmark and evaluated for BBB permeability (Pe) as reported in our previously published data (113). The calculated Pe values of all the tested compounds are presented in **Table 7.1**. On the comparison of threshold limit for BBB permeation established by *Di et al*., all the evaluated molecules anticipated their BBB permeability (CNS+) and can get to their respective targets certainly within the brain. Among all the tested derivatives, *N*-acetyl substituted pyrazoline containing phenyl ring substituted with electron withdrawing methoxy group (Compound **52**; *Pe* = 12.12 ± 0.728 × $10^{-6}$ cm $s^{-1}$) showed better BBB permeability. The potent ChEs inhibitors, compounds (**48**; *Pe* = 7.28 ± 0.474 × $10^{-6}$ cm $s^{-1}$ and **56**; *Pe* = 6.87 ± 0.444 × $10^{-6}$ cm $s^{-1}$) have appreciable BBB permeability.

### 7.3.4 *h*BACE-1 inhibition assay

To evaluate the multitargeting inhibitory activity of the designed compounds, the FRET-based *h*BACE-1 fluorometric assay was performed (185). Specifically, compounds (**48**, **53**, **54** & **56**) with dual potent AChE and BuChE inhibitory profile were selected for

further *in vitro h*BACE-1 inhibition studies (**Table 7.1**). Among all the evaluated compounds, para-bromo substituted compound **54** and unsubstituted compound **48** exhibited potent *h*BACE-1 inhibition at 10 μM of inhibitory concentration. Moreover, other compounds also showed the significant inhibitory potential against BACE-1 at inhibitory concentration. There was no significant alternation in the BACE-1 inhibitory potential was observed for the tested compounds than previously reported derivatives. Pertaining to the obtained *in vitro* results, compound **48** was selected as MTDL for further evaluation.

### 7.3.5 Self-induced and AChE-induced $A\beta_{1-42}$ aggregation

The current AD research also emphasizes on the inhibition of $A\beta_{1-42}$ aggregation which is considered as a promising strategy for an effective therapy of AD (214). Thioflavin T assay was performed to accompanied the anti-Aβ aggregation potential of optimal compound **48**. The experiments for compound **48** were carried out against both self- and AChE-induced $A\beta_{1-42}$ aggregation inhibition activity (**Figure 7.2**). Herein, three different ratios of concentrations of $A\beta_{1-42}$: compound **48** (10:5, 10:10, and 10:20 μM) were included, DPZ was taken as reference and the obtained results were shown in terms of normalized fluorescence intensity (NFI). It indicated the Aβ aggregation inhibition in the concentration-dependent manner in the self and AChE-induced experiments. The significant anti-aggregation profile shown by the compound **48** against $A\beta_{1-42}$ aggregation assay. The maximal inhibition activity was displayed at higher concentration of 20 μM (Aβ: Compound **48**, 10:20 μM) in both experiments of self- and AChE-induced aggregation. It demonstrated the significant effect of compound **48** on the $A\beta_{1-42}$ aggregation inhibition.

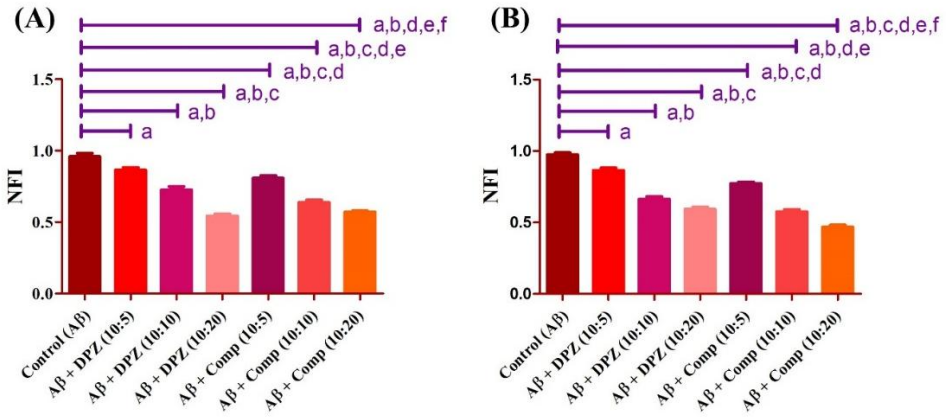


**Figure 7.2**. Thioflavin T assay of compound **48** to assess the modulation of $A\beta_{1-42}$ aggregation **(A)** Self-induced and; **(B)** AChE-induced. $^{a}p < 0.05$ vs. Control (Aβ), $^{b}p < 0.05$ vs. Aβ + DPZ (10:5), $^{c}p < 0.05$ vs. Aβ + DPZ (10:10), $^{d}p < 0.05$ vs. Aβ + DPZ (10:20), $^{e}p < 0.05$ vs. Aβ + comp 48 (10:5), $^{f}p < 0.05$ vs. Aβ + comp 48 (10:10). (One-way ANOVA followed by Newman - Keuls test).

### 7.3.6 Molecular docking analysis

The molecular docking studies were performed to gain insight into the interaction profile of compound **48** with proteins i.e., AChE (4EY7) and BACE-1 (2VKM) (215). Initially, the molecular docking protocol was validated and determined the ability to efficiently reproduce the pose similar to the co-crystallised ligand conformation with least deviation (187, 209). It displayed acceptable average RMSD deviations of 0.4128 Å of redocked donepezil against AChE. The active sites of the AChE mainly comprised of an esteratic site (Ser203, Glu334, and His447), anionic site (AS) (Trp86, Tyr133, Tyr337, and Phe338), and PAS, i.e., peripheral anionic site (PAS) (Tyr72, Asp74, Tyr124, Trp286, and Tyr341) (132, 216). Compound **48** has a chiral center, therefore docking studies were performed on both *R* and *S*-configuration of the molecule (217). The effective binding interaction profile shown by both (*R*) and (*S*)-enantiomers of compound **48** with the different residues of the PAS site, and the anionic site are presented in **Figure 7.3**. The binding energy and amino acid interactions have been accessed (**Table 7.2**). Docking studies on *R* and *S*-enantiomeric forms showed nearly similar interactions with the AChE.

The principle optimized *N*-acetyl pyrazoline scaffold of both *R* & *S* configuration of compound **48** displayed strong bonding interaction with Tyr337, an aromatic residue in the anionic sub-site of AChE that plays a role in the enzyme's catalytic reaction mechanism (218). Moreover, phenyl ring with attached pyrazoline scaffold of both *R* and *S* formed π-π stacking and π–sigma type interactions with Trp86 amino acid residue, respectively. Rest of the crucial part of the molecule including, *N*-benzyl piperazine **was** oriented towards the PAS site. The moiety formed the multiple binding interactions with PAS residues. Here, the common and crucial amino acids, Trp286 and Tyr341 displayed interaction with both *R* & *S* of compound **48**. Some distinct interaction was also been displayed by *R* & *S* configurations with other amino acid residue including, Leu289, Val294 and Tyr341. The binding energies (**Table 7.2)** for both enantiomers of compound **48 (**-12.11 kcal/mol, *R*; -12.32 kcal/mol, *S*) established that both forms of compound **48** probably act as potent inhibitors with nearly identical activity.

**Table 7.2:** Binding energy and amino-acids interactions of compound **48** with AChE.

| **Compound 48** | **Binding energy (kcal/mol)** | **Amino acid interactions** |
|---|---|---|
| ***R*** | -12.11 | H-bond (TYR337), π-π stacking (TRP86, TRP286), π-alkyl (LEU289), Unfavourable acceptor-acceptor bond (TYR341). |
| ***S*** | -12.32 | C-H bond (TYR341), π-sigma (TRP86), π-lone pair (TYR337, TYR341), π-π stacking (TYR124, TRP286), π-alkyl (VAL294) |

**Table 7.3:** Binding energy and amino-acids interactions of compound **48** with BACE-1.

| **Compound 48** | **Binding energy (kcal/mol)** | **Amino acid interactions** |
|---|---|---|
| ***R*** | -11.54 | C-H bond (ASP32, TYR198), π-alkyl (VAL69, TYR71, ILE126), unfavourable acceptor-acceptor (GLN73). |
| ***S*** | -11.60 | C-H bond (ASP32), π-alkyl interaction (LEU30, TYR71, ILE110, ILE126) |

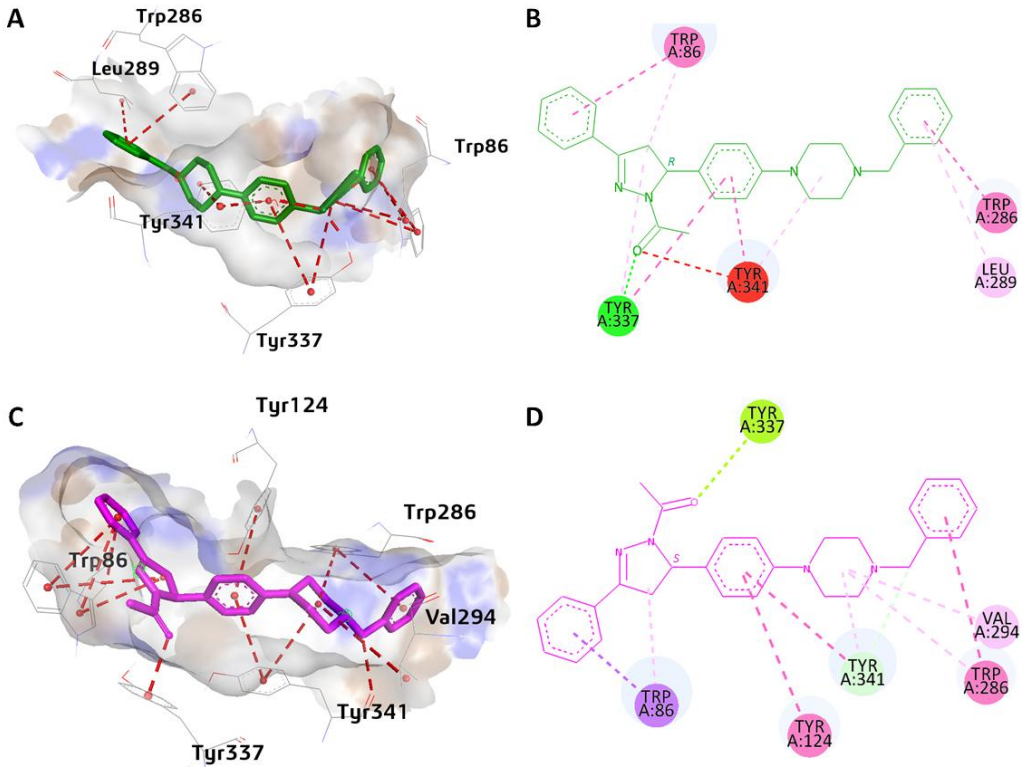


**Figure 7.3. (A, C)** Three-dimensional and **(B, D)** Two-dimensional binding mode of the compound **48** with active site of AChE (4EY7). (**A,B:** *R* and **C,D:** *S*).

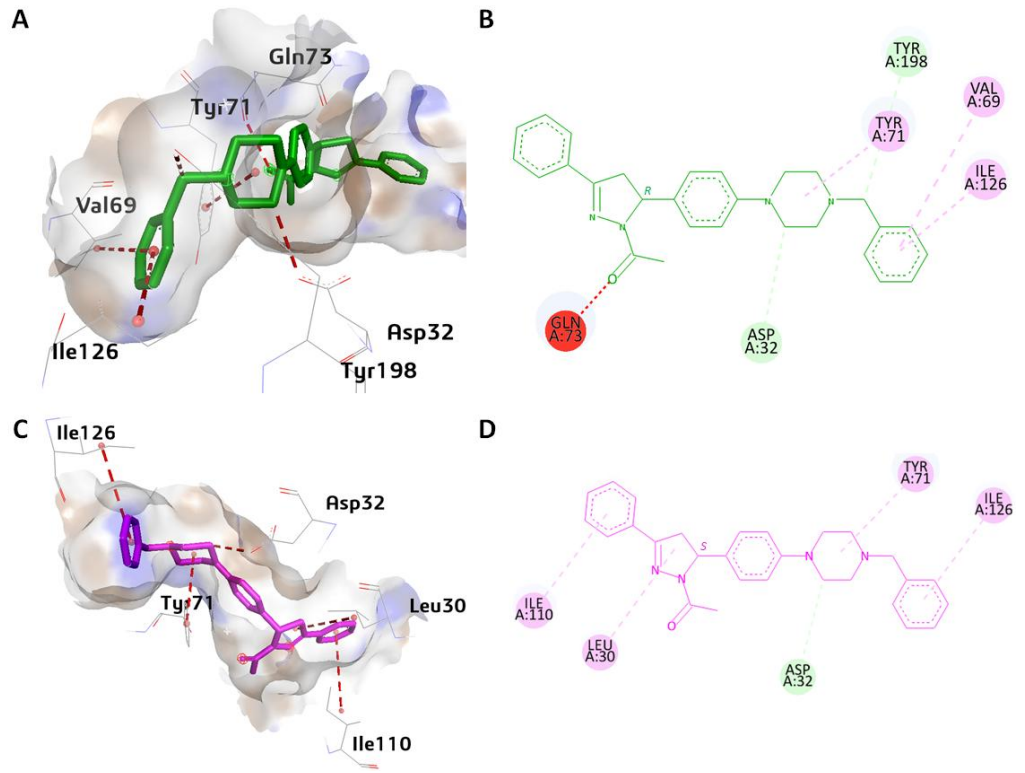


**Figure 7.4. (A) (A, C)** Three-dimensional and **(B, D)** Two-dimensional binding mode of the compound **48** with active site of BACE-1 (PDB ID: 2VKM) (**A,B:** *R* and **C,D:** *S*).

Furthermore, interesting binding mode interactions displayed by the *R* and *S*-forms of compound **48** with BACE-1 are included in **Figure 7.4**. Importantly, *N*-benzyl piperazine scaffold of both *R* & *S*-forms interacted with one of the aspartate residues that form the catalytic dyad in the active site of BACE-1 i.e., Asp32 with carbon-hydrogen type interaction (215, 219). The *R* & *S* of the molecule was also involved in the interaction with flap region residues, Tyr71 with π–alkyl bonding interaction. The *N*-benzyl piperazine moiety of *R*-form showed π-alkyl type interaction with Val69 and Ile126 and carbon-hydrogen interaction with Tyr198 amino acid residues. The phenyl ring along with attached pyrazoline scaffold of *S*-form showed π-alkyl type interaction with Ile110 and Leu30 (215). The lower binding energies (**Table 7.3)** for both enantiomers of compounds **48** against BACE-1 **(**-11.54 kcal/mol, *R*; -11.60 kcal/mol, *S*) was observed.

### 7.3.7 Molecular dynamics

The MD simulation is a widely used computational method for an in-depth analysis of the structural and confirmational changes in the system under the specified simulated physiological environment and binding interaction of the protein and ligand. The *R* & *S*-configurations of lead compound **48** were studied through MD simulation against AChE of 100 ns using GROMACS v2020. On the completion of the run, MD trajectories generated and different parameters such as RMSD, RMSF, RoG and SASA for both protein-ligand complex were studied. The protein-ligand complex of both *R* & *S* forms of compound **48** with AChE were analyzed. The RMSD plot of the protein (**Figure 7.5 A**) indicated the fluctuation between 0.15 to 0.25 nm in the overall simulation run. The slight hump shaped deviation occurred at around 20 ns but the stability was observed throughout the simulation time. The RMSD fluctuation for both *R* and *S* of the ligand throughout the simulation run was observed between 0.35 to 0.6 nm. However, *R*-form showed somewhat more sustained stability than *S*-form of the compound **48**. Where,

major fluctuation of *S*-form was observed at simulation run of 15 ns, 55 ns and 60 – 70 ns during 100 ns of total run time. The RMSF value of the ligand (**Figure 7.5 C**) of both forms of the compound **48** in complex with protein was found to be 0.05 to 0.25 nm indicating their flexibility and exertions to interact with protein atoms. The protein backbone showed slightly higher RMSF values up to 0.6 nm compared to the ligand RMSF. Moreover, the stability of the both *R* & *S* forms of protein-ligand complex was also accessed through the other parameters such as ROG (2.31 to 2.37 nm) and SASA (210 – 240 $nm^2$) and protein-ligand hydrogen bonding interaction throughout the simulation run of 100 ns.

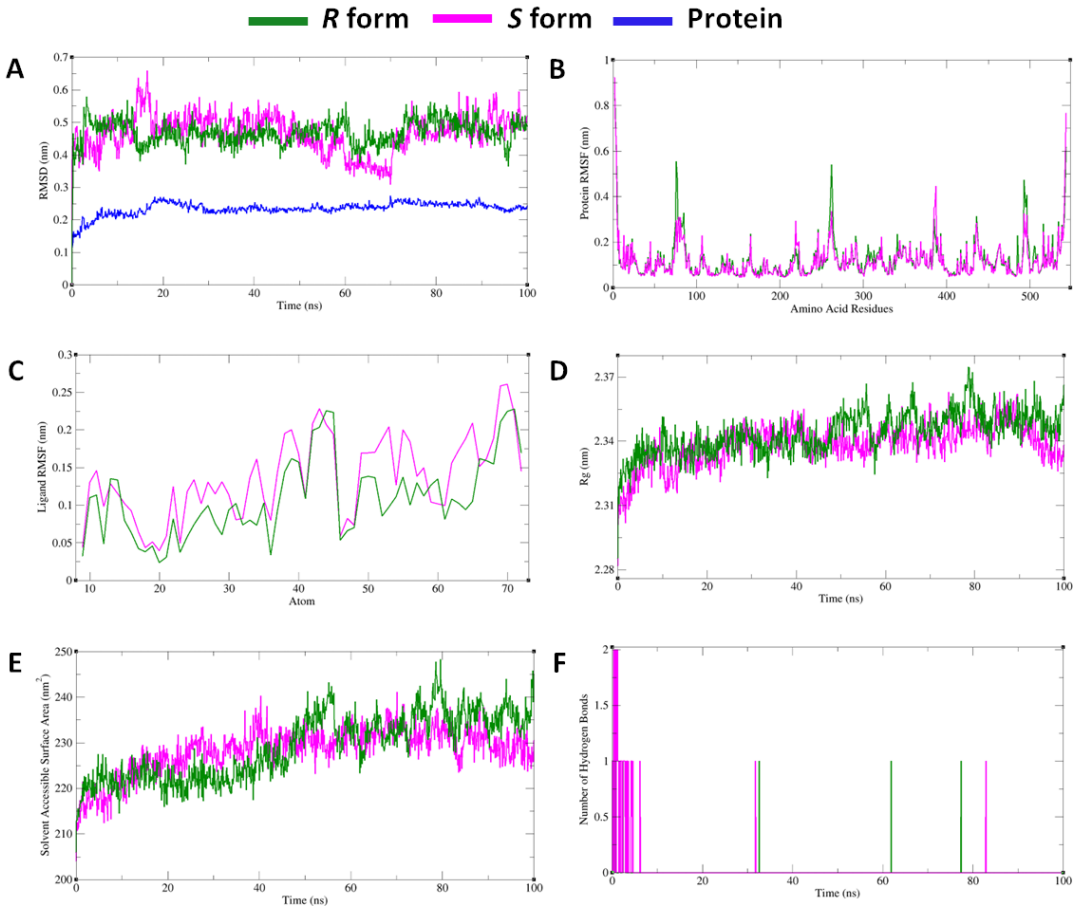


**Figure 7.5** MD simulation analysis of compound **48** (*R*- and *S*-form) with AChE (4EY7) docked ligand–protein complex **(A)** RMSD **(B)** Protein RMSF **(C)** Ligand RMSF **(D)** Radius of gyration (RoG) and **(E)** Solvent accessible surface area (SASA). **(F)** Number of intermolecular hydrogen bonds formed between protein-ligand complex throughout the simulation run of 100 ns.

### 7.3.8 *In vivo* biological evaluations

#### 7.3.8.1 Acute oral toxicity studies

The safety profile evaluation of optimal compound **48** was conducted according to OECD guideline 423 for acute oral toxicity in female mice. Findings indicated no adverse effects on behavior, body weight, consumption of food and water, nor any mortality following administration. Additionally, there was no significant histological damage observed in the tissues of the brain, liver, heart, or kidneys at doses up to 300 mg/kg. (**Figure 6)**.

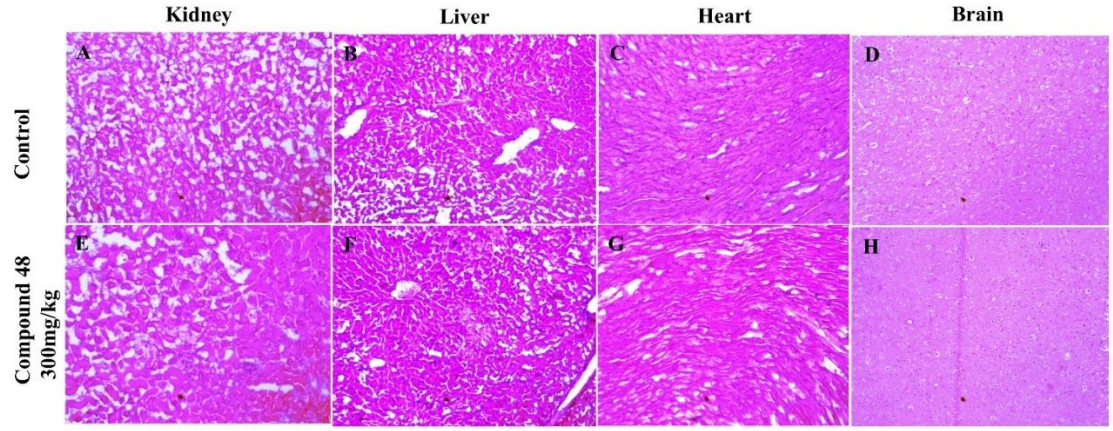


**Figure 7.6.** Histological analysis of major organs. (A–D) shows histological changes in the kidneys, liver, heart, and brain in the untreated control group. (E–H) illustrates the impact of compound 48 on histological changes in the kidneys, liver, heart, and brain, respectively.

#### 7.3.8.2 Behavioural studies

The *in vivo* therapeutic efficacy of compound **48** was assessed through behavioural studies to evaluate its potential in mitigating cognitive dysfunction and enhancing memory in a scopolamine-induced cognitive deficit mouse model (126). The percentage of alternation in memory impairment caused by scopolamine was measured after treatment with compound **48** by using the Y-maze test (151, 152). Spontaneous alternation behaviour was examined for doses of 5, 10, and 20 mg/kg of compound **48**, with DPZ (5 mg/kg) serving as a reference standard (**Figure 7.7**). The test recorded sequential arm entries and percentage of spontaneous alternations, along with total arm

entries for each animal. Significant differences were found across all groups, as shown by one-way ANOVA. A notable decrease in percentage alternation ($p < 0.05$) was observed in scopolamine-treated mice compared to the control group. However, groups treated with compound **48** showed significant increase in the percentage spontaneous alternation. Compound **48** at doses of 5, 10, and 20 mg/kg significantly improved the spontaneous alternation compared to the scopolamine group. Moreover, there were no significant differences ($p > 0.05$) observed by the group treated with dose of 10 and 20 mg/kg of compound **48** and relative to DPZ-treated mice. The obtained results indicated that compound **48** significantly enhanced cognitive and memory functions in the scopolamine-induced cognitive deficit model.

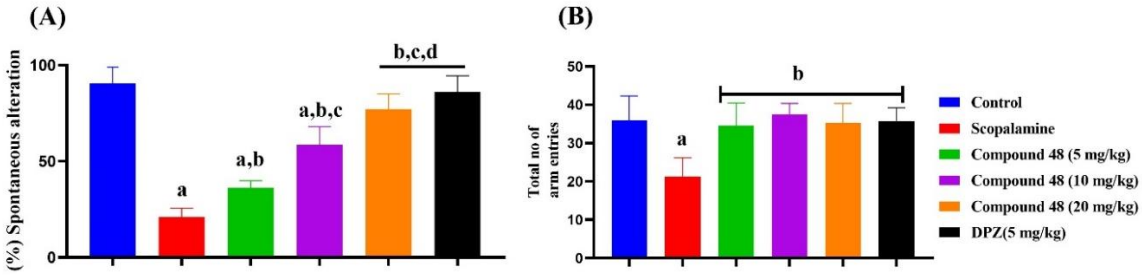


**Figure 7.7.** Effect of compound **48** and DPZ on cognition enhancement in scopolamine-induced Y-maze amnesia model. **(A)** Indicates the % spontaneous alternation. **(B)** Shows the total number of arm entries. Significance levels: a indicates $P < 0.05$ compared to control; b denotes $P < 0.05$ compared to scopolamine; c indicates $P < 0.05$ compared to compound **48** at 5 mg/kg; d represents $P < 0.05$ compared to compound **48** at 10 mg/kg. Statistical analysis was performed using one-way ANOVA followed by the Newman-Keuls post hoc test.

### 7.3.8.3 *Ex-vivo* biochemical analysis

The assessment of ACh and AChE activity, and other biochemical markers including MDA and CAT, demonstrated the neurochemical effects of compound **48**. Following the behavioural studies, mice from each group were decapitated, and the hippocampus region was isolated and homogenized. ACh levels were measured using an ELISA kit, while

AChE activity was determined with the Ellman assay (134). Results revealed that scopolamine-treated mice exhibited reduced ACh levels and increased AChE activity than that of the control group ($p < 0.05$). However, treatment with compound **48** significantly elevated ACh levels and reduced AChE activity as compared to the scopolamine group ($p < 0.05$). Additionally, the antioxidant effects of compound **48** were assessed through MDA and CAT levels. Scopolamine-treated mice showed significantly lower CAT and higher MDA levels relative to the control group ($p < 0.05$) (**Figure 7.8**). Treatment with compound **48** reduced MDA levels and significantly increased CAT levels as compared to the scopolamine group. The DPZ-treated group also showed increase in CAT and significantly reduced MDA ($p < 0.05$). The *ex vivo* biochemical findings suggested that compound **48** had AChE inhibitory properties and notable antioxidant potential.

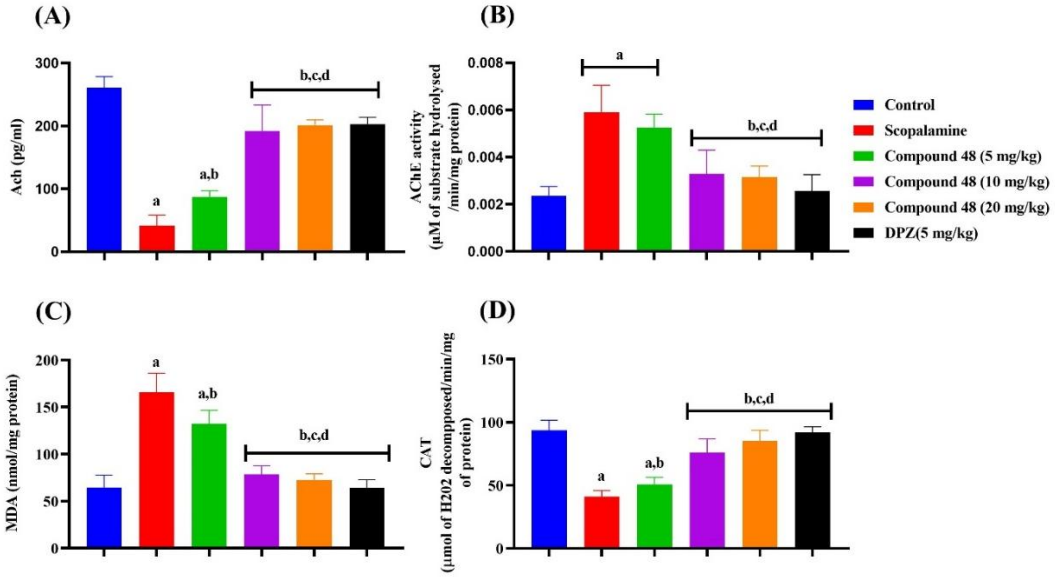


**Figure 7.8**. *Ex vivo* analysis of compound **48 (A)** ACh levels and **(B)** AChE levels in hippocampal brain **(C)** MDA level and **(D)** CAT activity. Data are expressed as mean ± SD (n = 6). [a] $P < 0.05$ vs. control; [b] $P < 0.05$ vs. scopolamine; [c] $P < 0.05$ vs. Compound **48** (5 mg/kg); [d] $P < 0.05$ vs. compound **48** (10 mg/kg). Statistical analysis was performed using one-way ANOVA followed by the Newman-Keuls post hoc test.

### 7.4 Summary and conclusion

In the present study, we have delineated the lead optimization-based strategy for the development of multi-targeted ligand for the treatment of AD. The chalcone scaffold was optimized to derive the pyrazoline series with different substituents at the *N*-aryl piperazine moiety. A series of twenty-five novel structural analogs of pyrazoline containing benzylpiperazine were synthesized (**32-57**). The preliminary *in vitro* biological evaluation against the major targets of AD, i.e., ChEs, BACE-1, and Aβ showed significant inhibitory potential and BBB permeability. Amongst all the tested derivatives, *1-(5-(4-(4-Benzylpiperazin-1-yl)phenyl)-3-phenyl-4,5-dihydro-1H-pyrazol-1-yl)ethan-1-one* (**48**, *ee*AChE $IC_{50}$ = 2.89 ± 0.706 μM; *eq*BuChE $IC_{50}$ = 0.151± 0.089 μM) possessed the most significant inhibitory profile. The SAR studies signified the importance of various structural features responsible for the inhibitory potency of the derivatives. Our findings outline that the presence of the *N*-acetylation on pyrazoline scaffold bearing *N*-benzylpiperazine fragment exhibited potent inhibitory activity. Additionally, compound **48** also showed a remarkable inhibitory potential against *h*BACE-1. The optimal binding orientation was shown by *R* & *S*-configuration of lead compound **48** with AChE and BACE-1 in molecular docking studies. The protein–ligand complex stability of both configuration against AChE was evaluated with MD simulation studies. At 20 μM, compound **48** exhibited maximal anti-$A\beta_{1-42}$ aggregation potential in self-induced and AChE-induced assays, which indicated the multi-targeting potential of lead compound **48**. Moreover, compound **48** demonstrated dose-dependent increase in % spontaneous alternations in scopolamine-induced amnesic model. In Y-maze test, the compound, at a dose of 20 mg/kg, produced significant reversal of learning and memory functions. The data of *ex-vivo* analysis showed significant reduction in the AChE and an increase in levels of ACh. The assessment of oxidative biochemical markers including MDA and CAT showed the antioxidant potential of test compound **48**. The attenuated

levels of MDA and CAT were observed with the treatment of lead compound **48**. Overall findings advocated compound **48** to be the most promising multi-target directed ligand and led us to report it as a promising and effective lead for the treatment of AD.